POINT DEFECTS AND CAPTURE OF IMPURITIES IN CRYSTALS

Keshra Sangwal
LUBLIN UNIVERSITY OF TECHNOLOGY

I. Introduction to defects
II. Types of point defects
III. Statistics of point defects
IV. Diffusion in crystals
V. Methods for creation of point defects
VI. Point defects during crystal growth
VII. Capture of impurities in crystals

- Distribution coefficient of impurities
- Equilibrium segregation coefficient
- Effective segregation coefficient k_{eff}
- Relationship between k_{eff} and face growth rate R
- Threshold supersaturation for trapping of impurities during crystal growth

I. Introduction to defects

Perfect or ideal crystal lattice – arrangement of points in 3D space

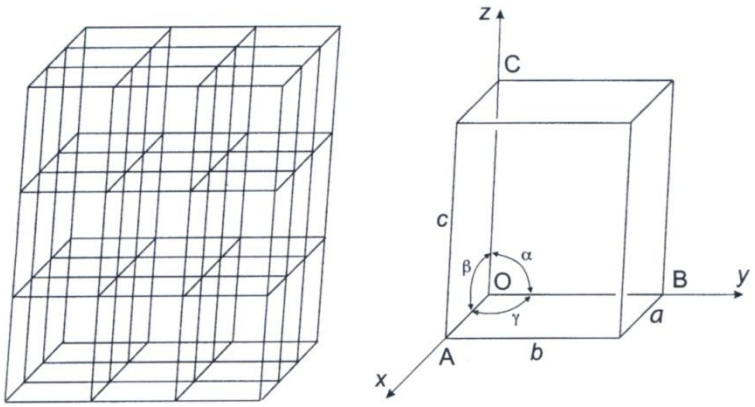

(a) (b)

Figure 1.1 (a) A space lattice, (b) unit cell showing positions of principal axes.

- **Concept of ideal crystal useful to explain -**

Some of the properties of crystals (for example: density, specific heat, and dielectric susceptibility, independent of details of crystal structure.

No real crystal is ideal –

Contains faults or flaws (known as defects or imperfections).

Many properties of crystals (e.g. mechanical strength, electric conductivity, mangetic hysteresis, etc.) are very sensitive to the extent of imperfections in them.

Type of defects in crystals

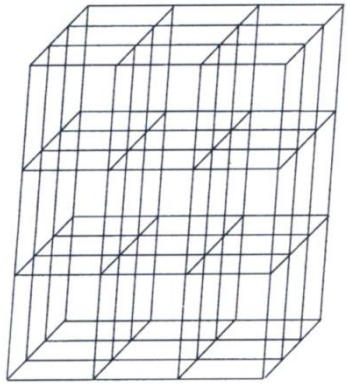

- **Thermal vibrations of atoms**

0 **Point defects**

vacancies, interstitial atoms, and impurity atoms (chemical contamination)

1 **Line defects**

Dislocations: edge, screw, and mixed

2 Planar defects

External surfaces of crystals, internal surfaces in crystals (grain boundaries, twin boundaries, and stacking faults)

3 **Volume defects**

II. Types of point defects: examples

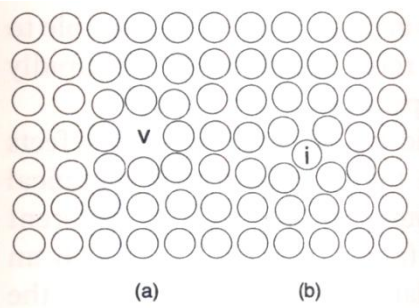

Figure 1.10 (a) Vacancy, (b) self-interstitial atom in an (001) plane of a simple cubic lattice.

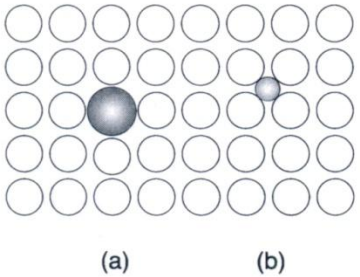

Figure 1.11 (a) Substitutional impurity atom, (b) interstitial impurity atom.

Metals

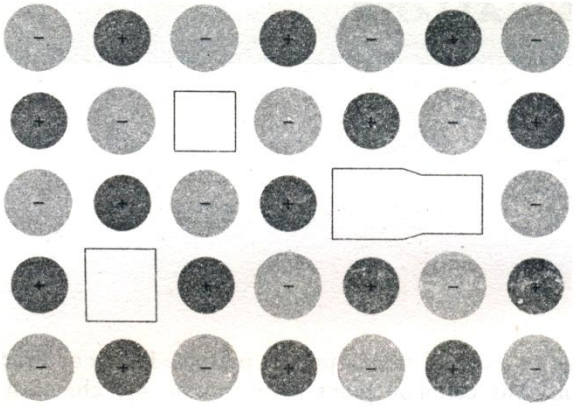

Figure 1 A plane of a pure alkali halide crystal, showing a vacant positive ion site, a vacant negative ion site, and a coupled pair of vacant sites of opposite sign.

1:1-type ionic crystal

Missing points and/or displacement of missing points to interstitial sites

Schottky and Frenkel defects

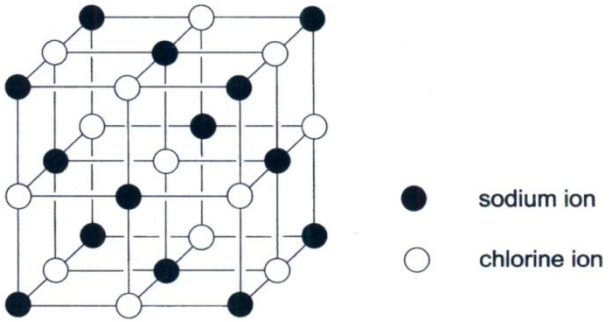

Figure 1.12 Sodium chloride structure which consists of two interpenetrating face-centred cubic lattices of the two types of atom, with the corner of one located at the point $\frac{1}{2}$, 0, 0 of the other.

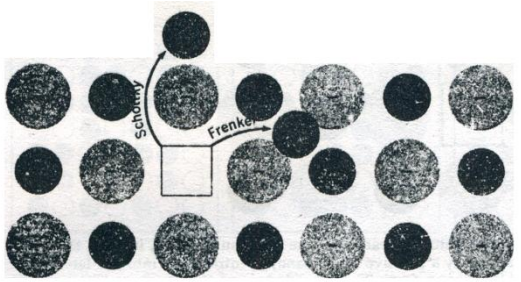

Figure 2 Schottky and Frenkel defects in an ionic crystal. The arrows indicate the displacement of the ions. In a Schottky defect the ion ends up on the surface of the crystal; in a Frenkel defect it is removed to an interstitial position.

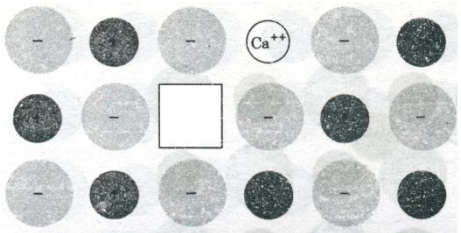

Figure 3 Production of lattice vacancy by the solution of $CaCl_2$ in KCl: to ensure electrical neutrality a positive ion vacancy is introduced into the lattice with each divalent cation Ca^{++}. The two Cl^- ions of $CaCl_2$ enter normal negative ion sites.

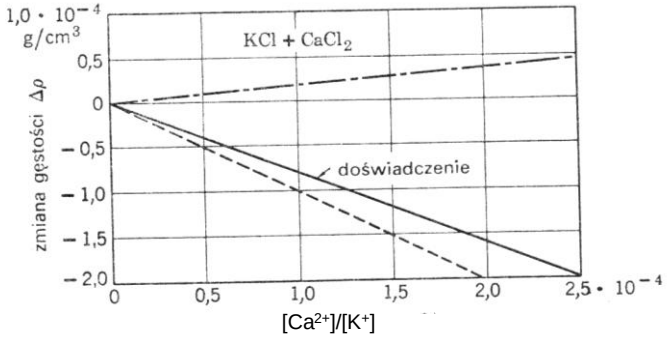

Change in the density ρ of KCl with $CaCl_2$ concentration.

Example:
KCl:$CaCl_2$

From Kittel .

III. Statistics of point defects

A.J. Dekker, Solid State Physics, MacMillan, London (1964).

Natural source of point defects

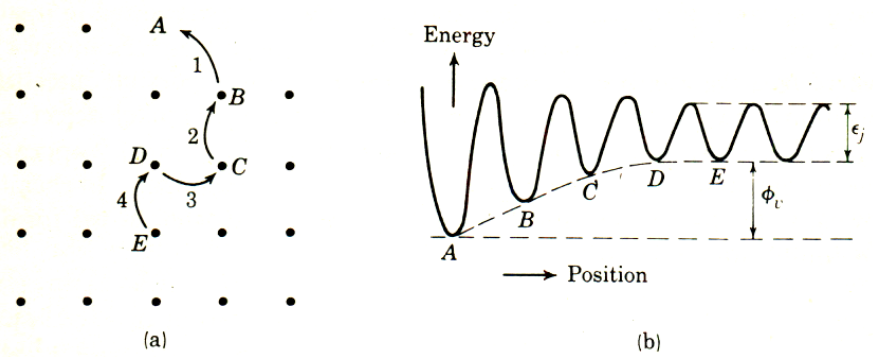

Fig. 3-5. Sequence of jumps producing a vacancy which migrates into the interior of the crystal (a). In (b) the potential energy of the vacancy is shown schematically as it diffuses in; the limiting value ϕ_v is the energy of formation, ε_j is the jump activation energy of the vacancy.

- Presence of phonons
- Absorption of phonons

ε_j – jump activation energy of vacancy

ϕ_v – energy for creation of vacancy (= E_v)

If E is the total energy to separate all N crystal atoms from each other, the sublimation energy per atom is: $\varepsilon_s = E/N$.

For an atom of potential energy ε_i in the interior of the crystal, the dissociation energy of the crystal is $N\varepsilon_i/2$.

Obviously, $\varepsilon_s = \varepsilon_i/2$.

Therefore, the energy $\phi_v = E_v$ required to transfer an atom from the interior to the surface (i.e. to form a vacancy) is:

$$\phi_v = \varepsilon_i - \varepsilon_r - \varepsilon_s = \varepsilon_s - \varepsilon_r,$$

For Cu metal, ε_s = 3.5 ev.

With $\phi_v = \phi_r$, this gives

$\phi_v \approx 1.7$ ev = 170 kJ/mol

Observed $\phi_V \approx 1.4$ ev,

$\varepsilon_j \approx 0.5$ ev = 50 kJ/mol

Thermal equilibrium

A.J. Dekker, Solid State Physics, MacMillan, London (1964).

Concentration (fraction) of vacancies

Thermodynamic parameters for a system:
Thermal free energy
or Helmholtz free energy: F
Internal energy: E
Entropy of the system: S

Equation for free energy:
$F = E - TS.$
Change in system free energy:
$\Delta F = \Delta E - T\Delta S.$

$\Delta E = nE_v\,(1 - \alpha T)$,
$\Delta S = \Delta S_{cf} + \Delta S_{th,}$
where:
$\Delta S_{cf} = k_B \ln[(N+n)!/N!n!]$,
$\Delta S_{th} = 3zk_B \ln(\nu/\nu')$

where:
N – normal lattice sites
n - number of defects
$(3N–3nz)$ oscillators of frequency ν
$3nz$ oscillators of frequency ν'
z – number of atoms surrounding a vacancy

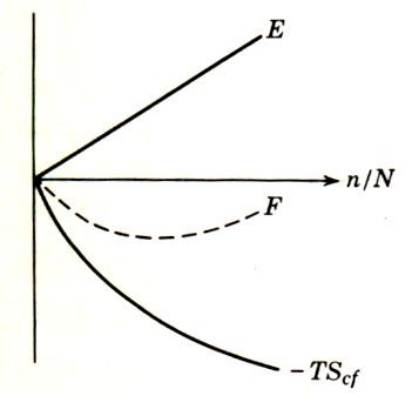

Fig. 3-4. Schematic representation of the energy and the configurational entropy term as function of the fraction of vacant lattice sites n/N. The minimum of the free energy F determines the equilibrium value of n/N.

We use Stirling's formula for $x >> 1$: $\ln x! = x\ln x$.

For metals:

$$\frac{n}{N+n} = \exp\left(\frac{\Delta S_{th}}{k_B}\right)\exp\left(\frac{\alpha E_v}{k_B}\right)\exp\left(-\frac{E_v}{k_B T}\right).$$

Handbook equation

$$n \approx N\exp(-E_v / k_B T).$$

Two parameters:
E_v and T

Concentration of other defects

Concentration of Frenkel defects in metals:

$$\frac{n}{(NN')^{1/2}} = K \exp\left(-\frac{E_F}{2k_B T}\right).$$

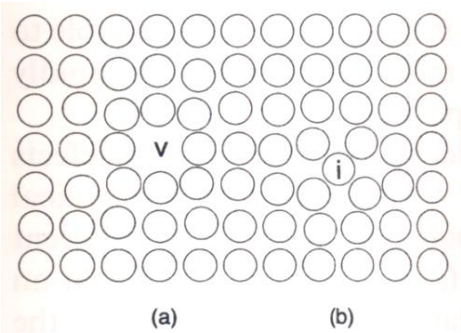

Figure 1.10 (a) Vacancy, (b) self-interstitial atom in an (001) plane of a simple cubic lattice.

Concentration of Schottky defects in ionic crystals:

$$\frac{n}{N} = K \exp\left(-\frac{E_p}{2k_B T}\right).$$

n - number of defects
N – normal lattice sites
N' - interstitial sites

Origin of Factor 2 ?

IV. Diffusion in crystals

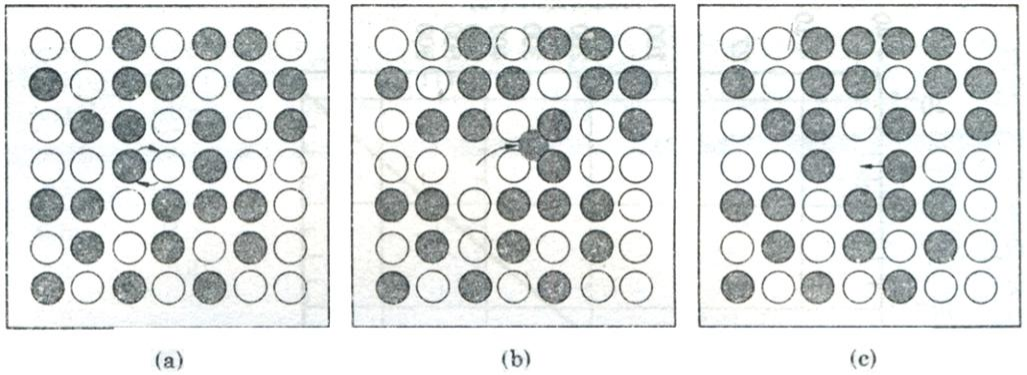

Figure 4 Three basic mechanisms of diffusion: (a) Interchange by rotation about a midpoint. More than two atoms may rotate together. (b) Migration through interstitial sites. (c) Atoms exchange position with vacant lattice sites. (From Seitz.)

Diffusion coefficient *D* in vacancy diffusion

$$D = \nu\delta^2 \exp\left(-\frac{E_v + \Delta H_m}{R_G T}\right)$$

Diffusion coefficient *D* in interstitial diffusion

$$D = \nu\delta^2 \exp\left(-\frac{\Delta H_m}{R_G T}\right)$$

ν - jump frequency
δ - jump distance
$R_G = k_B N_A$ - gas constant
ΔH_m – enthalpy of melting
ΔH_b – enthalpy of boiling

Estimation of some energies

For evaporation: Trouton rule

$$\Delta H_b \approx 10 R_G T_b$$

For melting: empirical trend

$$\Delta H_m \approx \xi R_G T_m$$

with the factor
$\xi = 2$, for metals;
$\xi = 3$, for inorganic salts.

For Cu,
$T_b = 2835$ K, $T_m = 1358$ K,
one obtains
$\Delta H_b = 235.7$ kJ/mol = 2.4 eV
$\Delta H_m = 33.9$ kJ/mol = 0.34 eV
$\varepsilon_s = \Delta H_m + \Delta H_b = 2.74$ eV

V. Methods for creation of point defects

1. Quenching from high temperature
2. Strong deformation i.e. plastic treatment (forging or rolling)
3. Bombardment by ions or high-energy charged particles
4. Growth processes (doping)

Two modes:
- Energy supplied by different means: thermal, mechanical, energy transfer
- structural changes

VI. Point defects during crystal growth

Mechanism: Structure of elementary steps

Rough steps:
- vacancies,
- impurities.

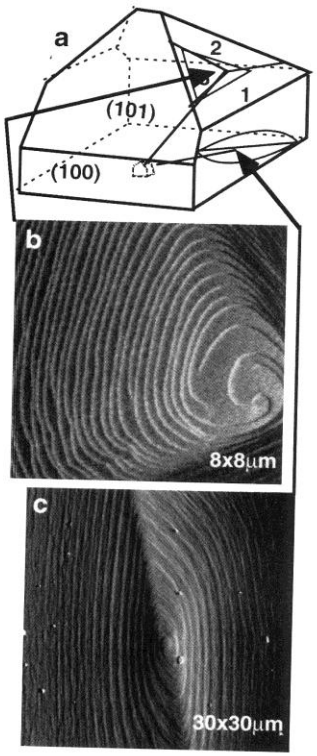

Figure 6. Example of KDP crystal surfaces preserved by pulling through hexane. (a) shows schematic of crystal structure. (b and c) Growth hillocks on the (b) {101} and (c) {100} face generated by dislocations emanating from the seed crystal interface.

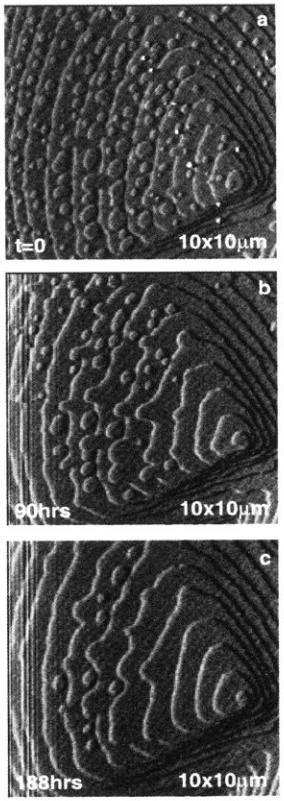

Figure 9. Coarsening of islands and steps on KDP {101}. With time, the material from the islands diffuses to the steps which in turn exhibit smoothing.

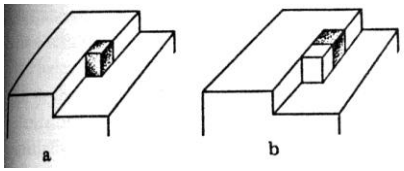

Fig.4.8a,b. Consecutive acts of entrapment of an impurity particle (*shaded cube*) during the building of a row with host particles (*open cubes*)

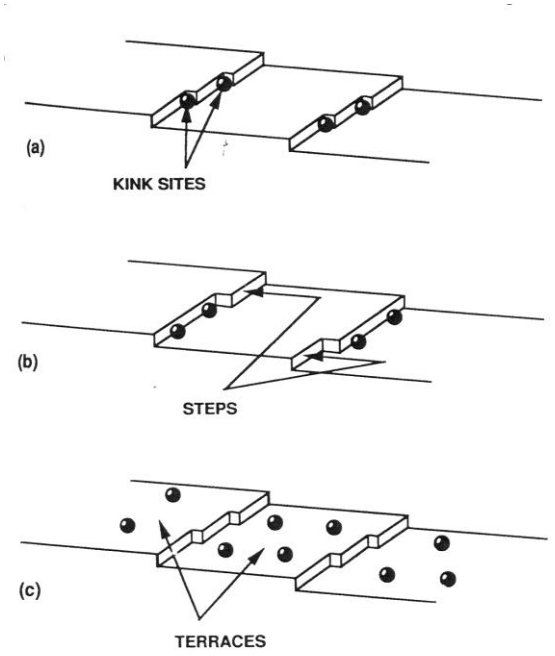

Figure 3.5 Key surface structures on an idealized crystal face: (a) kinks; (b) steps; and (c) terraces. Adsorbed impurities at each of these sites is illustrated. (Reproduced with permission from Mullin 1980.)

J.J. De Yoreo et al., in: Advances in Crystal Growth, Eds. K. Sato et al., Elsevier, 2001, p. 361-380.

Examples of images of segregation of impurities

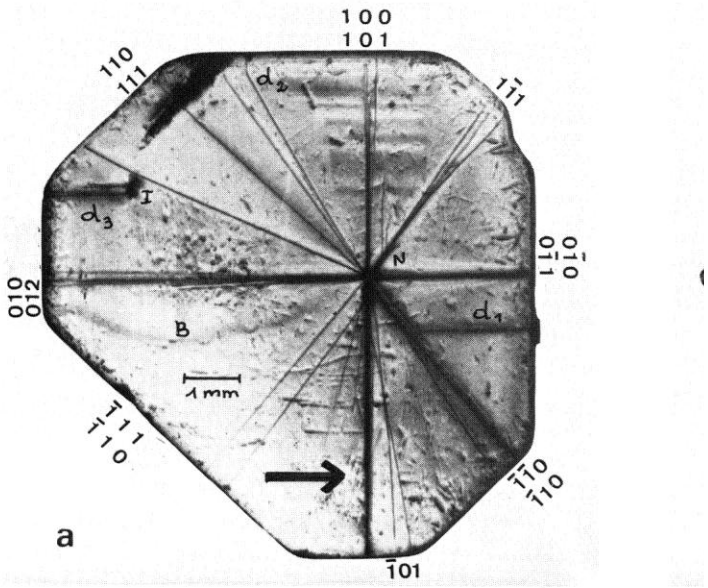

Fig. 6. Topographs of the two (010) slices cut out of an as grown KBC crys slice, ref. 120; MoK α.

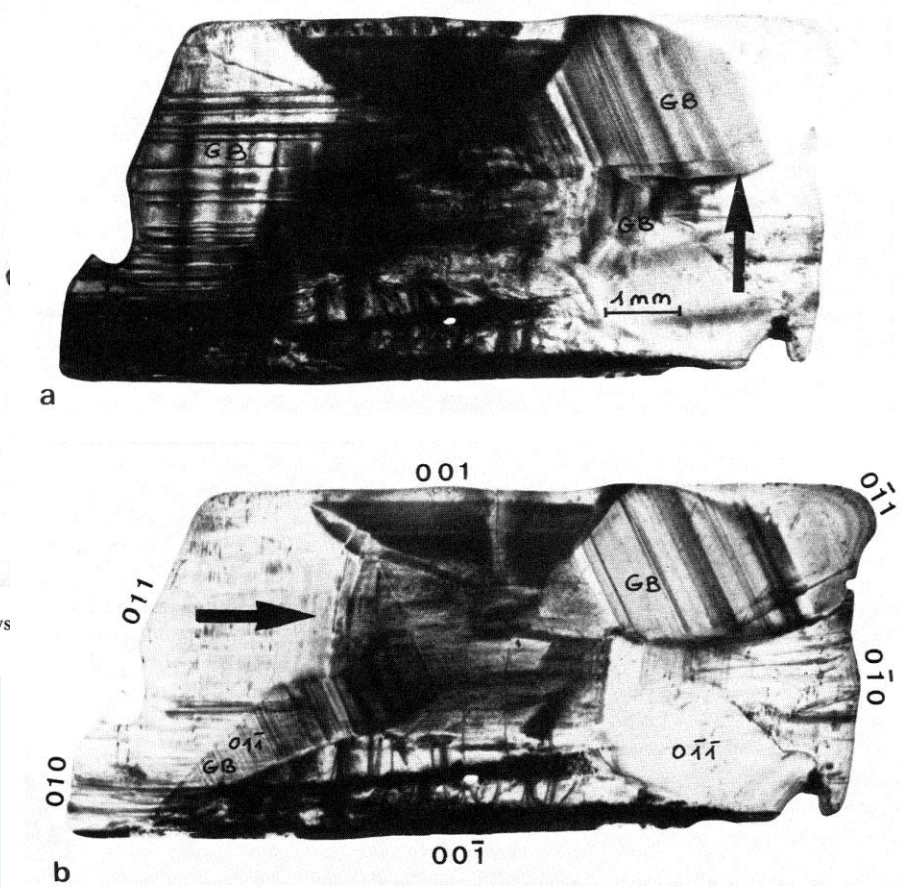

Fig. 8. Topographs of an as grown KBC crystal obtained at 47 °C in an aged solution: (a) ref. 020; (b) ref. 200; MoK α.

Sectorial nonuniformity as a result of different trapping in different growth sectors

Zonal nonuniformity in the same sector due to nonuniform growth rate

- Growth bands or
- Impurity striations

Examples and comments

Segregation coefficient *k* depends on structure and difference in size of atoms, ions and molecules in the common crystal lattice.

TABLE 2.4

Segregation coefficients in alkali halides†

Host	Solute	Segregation coefficient	
		Aqueous solution	Melt
NaCl	Li	0.007 ± 0.004	$0.21, 0.20 \pm 0.05, 0.19$
	K	0.005 ± 0.001	$0.20, 0.008 \pm 0.003$
	Br	0.047 ± 0.005	0.6
	I	$< 4 \times 10^{-4}$	0.06
KCl	Na	$< 6 \times 10^{-4}$	$0.03, 0.11 \pm 0.02, 0.31$
	Rb	0.113 ± 0.005	$0.68, 0.6 \pm 0.1, 0.70$
	Cs	0.0040 ± 0.0006	0.16, 0.21
	Br	0.189 ± 0.003	0.75, 0.71
	In	< 0.001	0.14
KBr	Rb	0.334 ± 0.004	$0.78, 0.4 \pm 0.1, 0.75$
	Cl	0.453 ± 0.005	0.86, 0.85
	I	0.039 ± 0.004	0.5, 0.52
KI	Rb	0.82 ± 0.03	0.76 ± 0.02
	Cs	0.03 ± 0.01	0.31 ± 0.01
	Cl	0.015 ± 0.02	0.39 ± 0.02
	Br	0.42 ± 0.02	0.79 ± 0.02
	NO_3	0.071 ± 0.004	0.43 ± 0.01

† Based on the data of Andreev (1967, 1969), Ikeya *et al.* (1968) and Gross (1970a, b).

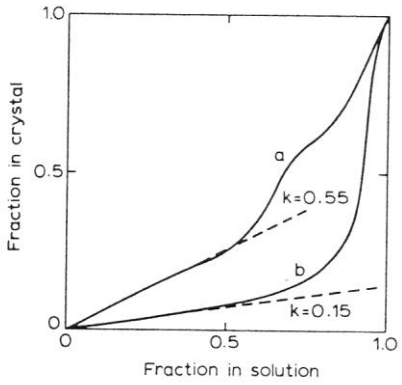

Fig. 2.20. The fractions in the solid and in aqueous solution of (a) copper sulphate and (b) ammonium sulphate in mixed crystals with potassium sulphate.

Brice (1973)

VII. Capture of impurities in crystals

Podstawowa literatura:
K. Sangwal, *Addititives and Crystallization Processes: From Fundamentals to Applications*, Wiley, Chichester, 2007, chap. 9.

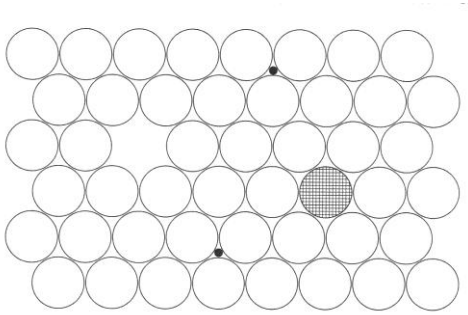

Figure 9.1 Different types of point defects involved during impurity incorporation: vacant site, substituted atom (hatched circle), and interstitial atoms (small black circles)

Large deformation of lattice does not favor capture of impurity atoms in it.

Impurities captured in crystal lattice are:

1) individual atoms, ions, molecules or complexes of molecular dimensions like dimers and trimers; uniform impurity capture. Solid solution is formed when $c_{iSolid} = c_{iLiquid}$ (thermodynamically equilibrium capture of impurities) or $c_{iSolid} \neq c_{iLiquid}$ (nonequilibrium impurity capture).

• Colloidal inclusions of micrometer dimensions; nonuniform capture of impurities.

Concentration and distribution of uniform and nonuniform capture of an impurity are different in the crystal volume due to thermal nonequilibrium at crystal-liquid interface.

Nonuniform capture occurs:

1) in different growth sectors of a crystal (sectorial nonuniformity),
2) In a given growth sector (zonal nonuniformity; growth bands, impurity striations),
3) In the vicinity of structural defects such as dislocations and grain and twin boudaries as enrichment or depletion of impurity (structural nonuniformity).

Distribution coefficient of impurities

Concentrations [C] and [A] in atomic/ionic fraction, weight fracrion or as mass in volume.

When impurity C (i) enters the substance A (s): segregation coefficient

$$k_d = \frac{[C_{solid}]}{[C_{solid}]+[A_{solid}]} \times \frac{[C_{liquid}]+[A_{liquid}]}{[C_{liquid}]}. \quad (1)$$

When [C] << [A],

$$k_d = \frac{[C_{solid}]}{[C_{liquid}]} \frac{[A_{liquid}]}{[A_{solid}]}. \quad (2)$$

In the case of growth from the melt

$$k_d \approx \frac{[C_{solid}]}{[C_{liquid}]}. \quad (3)$$

When concentration is in mole fraction

$$k_d = \frac{x_{iS} / x_{sS}}{x_{iL} / x_{sL}}. \quad (4)$$

S – solid
L - liquid

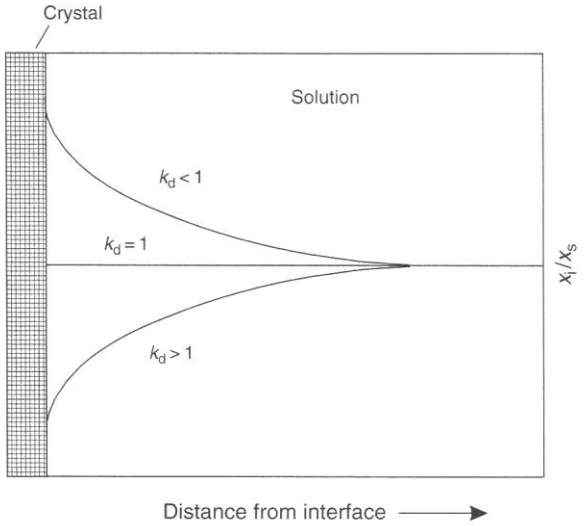

Figure 9.2 *Schematic illustration of the dependence of x_{iL}/x_{sL} on distance from the crystal–solution interface, and relationship between x_{iL}/x_{sL} at the crystal–medium interface and the segregation coefficient k_d. Adapted from Rimstidt et al. (1998)*

k_0 depends on physico-chemical properties of crystal and impurity.
k_{eff} depends on the nature of crystal-fluid interface; k_{eff} (smooth interface) < k_{eff} (rough interface).

Segregation of impurities

1. Equilibrium (supersaturation $\sigma \Rightarrow 0$)
   Equilibrium segregation coefficient k_0
2. Nonequilibrium ($\sigma > 0$)
   Effective segregation coefficient k_{eff}

Equilibrium segregation coefficient

1) Two-component mixture approach:

For C to enter A the theoretical description is similar to that of phase diagrams for two-component systems

In the case of C in A:

$$\ln k_0 = \frac{\Delta H_m^A}{R_G}\left(\frac{1}{T} - \frac{1}{T_m^A}\right) - \frac{\Delta H_m^C}{R_G}\left(\frac{1}{T} - \frac{1}{T_m^C}\right).$$

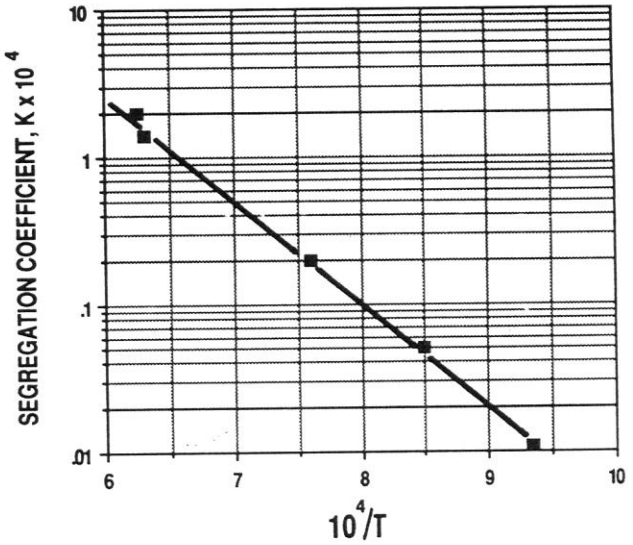

Figure 3.7 Logarithm of the segregation coefficient versus $1/T$ for copper in silicon crystals. (Reprinted with permission from C.D. Thurmond and J.D. Struthers (1953), *J. Phys. Chem.* 57, 831–835. Copyright 1953 American Chemical Society.)

2) Thermodynamic approach:

$$\ln k_0 = \ln k_0(0) - \Delta G / R_G T.$$

where: $k_0(0)$ is the value of k_0 when $r_i = r_s$, and ΔG is the change in the difference in the free energy.

Other approaches are based on: difference in volumes, heat of sublimation, diffusion coefficient, etc.

In the case of mismatch of volume fraction $\Delta V/V_A$ at a given temperature:

$$\ln k_{eq} = B_1 + B_2 \Delta V / V_A$$

$$= A - B + B(r_i / r_s)^3.$$

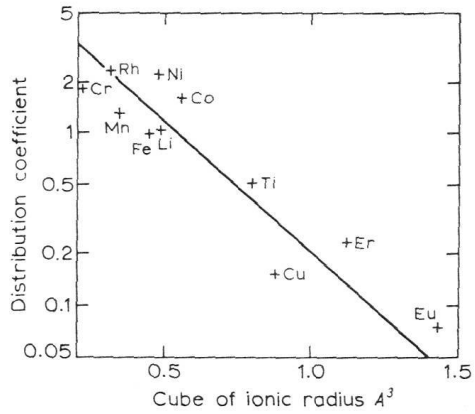

Fig. 2.21. Distribution coefficients in zinc tungstate as a function of the cube of the ionic radius.

When change in free energy is due to mismatch (r_i-r_s) of sizes of atoms/ions:

$$\ln k_0 = \ln k_0(0) - \frac{4\pi E N_A}{R_G T}\left(\frac{1}{2} r_s (r_i - r_s)^2 - \frac{1}{3}(r_i - r_s)^3\right),$$

where E – Young's modulus.

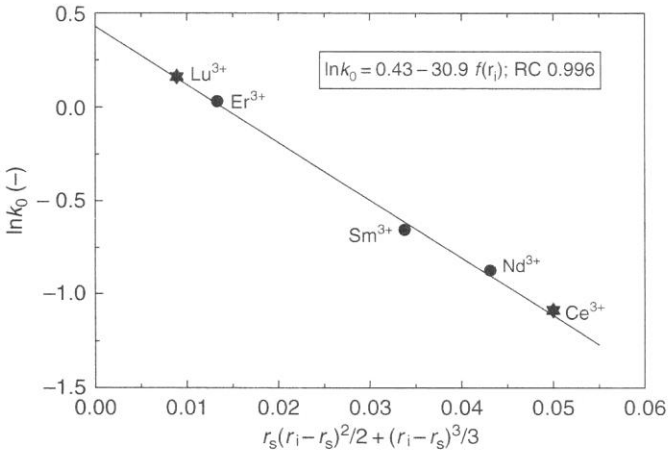

Figure 9.5 *Logarithm of equilibrium segregation coefficient k_0 of various rare earths in cubic ZrO_2 stabilized with Y_2O_3 as a function of $\frac{1}{2}r_A(r_i - r_s)^2 + \frac{1}{3}(r_i - r_s)^3$. Data for Er^{3+}, Sm^{3+}, and Nd^{3+} are experimental, whereas those for Lu^{3+} and Ce^{3+} are calculated from Equation (9.24). Adapted from Römer* et al. *(1994)*

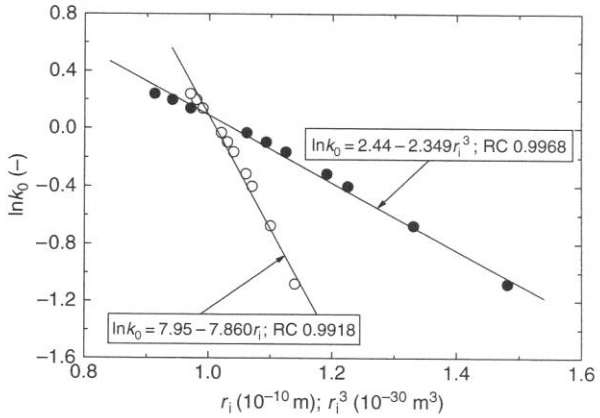

Figure 9.6 *Logarithm of equilibrium segregation coefficient k_0 of various rare earths in cubic ZrO_2 stabilized with Y_2O_3 against additive cationic radii r_i and r_i^3. The cationic radii r_i and r_i^3 are due to Shannon, with coordination number 8. Data from Römer* et al. *(1994)*

Some more examples

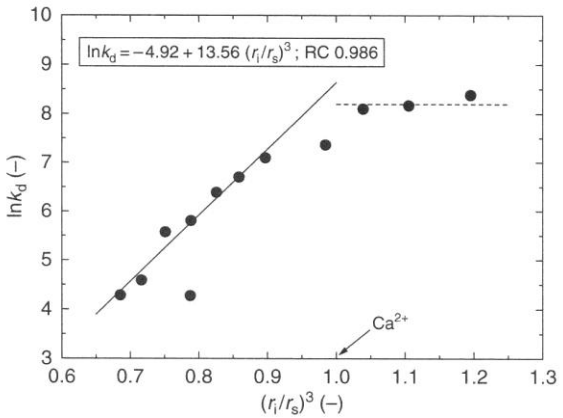

Figure 9.8 *Logarithm of k_d for various trivalent rare earth metal ions in calcite as a function of $(r_i/r_s)^3$. The effective ionic radius, due to Shannon, is in six-fold coordination. The extremely deviating point for $(r_i/r_s)^3 = 0.78$ was excluded while fitting the data. Data from Rimstidt* et al. *(1998)*

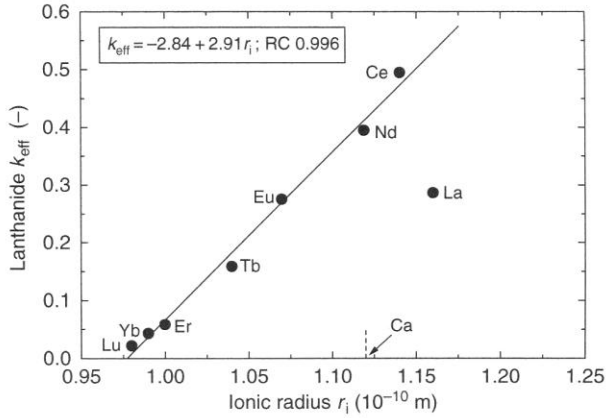

Figure 9.9 *Plot of k_{eff} for various lanthanide ions in gypsum crystals against their radii r_i. Data from de Vreugd* et al. *(1994)*

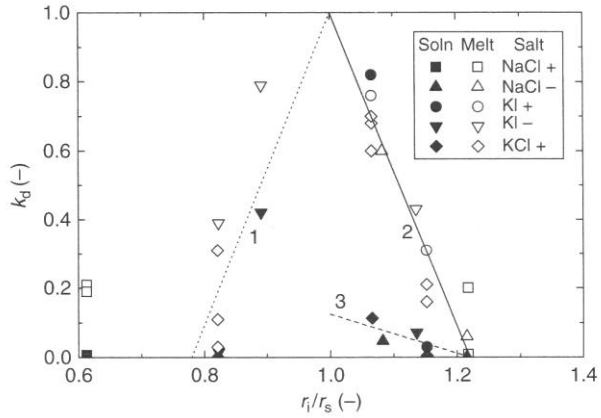

Figure 9.10 *Dependence of segregation coefficient k_d of cations and anions in different alkali metal halides grown from aqueous solutions and from the melt on their Shannon radii r_i, with coordination number 8 or 9. Data from Brice (1973). Additive cations and anions are denoted by + and –, respectively, in the inset*

Effective segregation coefficient

1) Bulk diffusion model of Burton et al. (1953):

$$k_{eff} = \frac{k_0}{k_0 + (1 - k_0)\exp(-R\delta / D)}, \qquad (1)$$

where: δ - thickness of diffusion layer,
D – diffusion coefficient of impurity in the solution.

For $k_0 << 1$

$$k_{eff} = k_0 \exp(R\delta / D) \qquad (2)$$

From the plots
δ/D = 30 – 150 s/m.

Since $D = 10^{-12} – 10^{-9}$ cm^2/s,
δ = 0.3 – 1.5 nm.

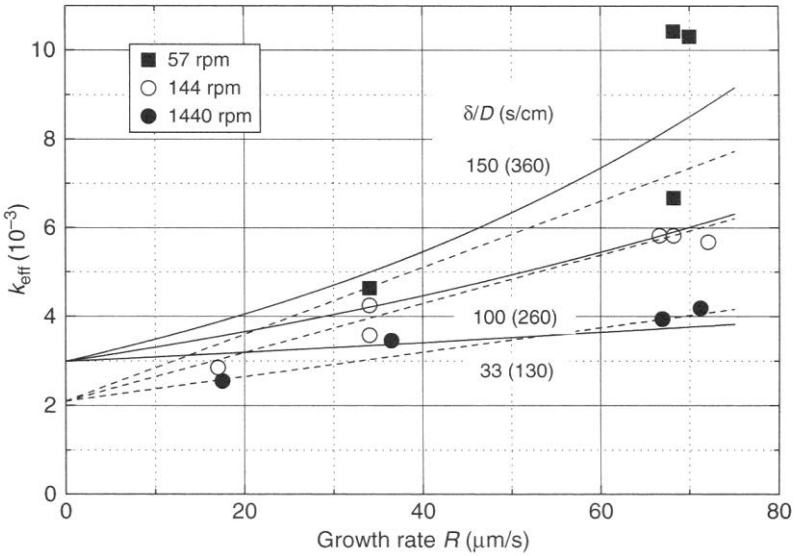

Figure 9.11 *Dependence of segregation coefficient k_{eff} of Sb in Ge crystals on growth rate R for different stirring conditions. Solid curves were drawn according to the BPS Equation (9.26) due to Burton* et al. *(1953), and dashed lines are according to the linear dependence in Equation (9.28). The values of δ/D for the linear dependence are given in parentheses. Adapted from Burton* et al. *(1953)*

2) Approach involving diffusion-relaxation

Hall (1953), Kitamura and Sunagawa (1977), and Chernov (1984):

$$k_{eff} = k_0 + (k_{ads} - k_0)\exp(-R_i / R), \quad (1)$$

with

$$R_i = h / \tau$$

where:
h – thickness of step on growing surface,
τ - time interval for the growth of successive layers,
k_{ads} – segregation coefficient of the impurity in the adsorption layer.

When $k_0 << 1$,

$$k_{eff} = k_{ads}\exp(-R_i / R), \quad (2)$$

and when $R_i/R << 1$,

$$k_{eff} = k_{ads} - k_{ads}(R_i / R). \quad (3)$$

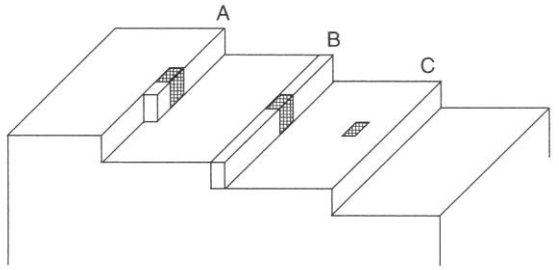

Figure 9.12 *Different positions of trapped impurity particles: (A) trapped in a kink, (B) trapped in a step ledge by solute particles from both sides, and (C) trapped in the surface terrace*

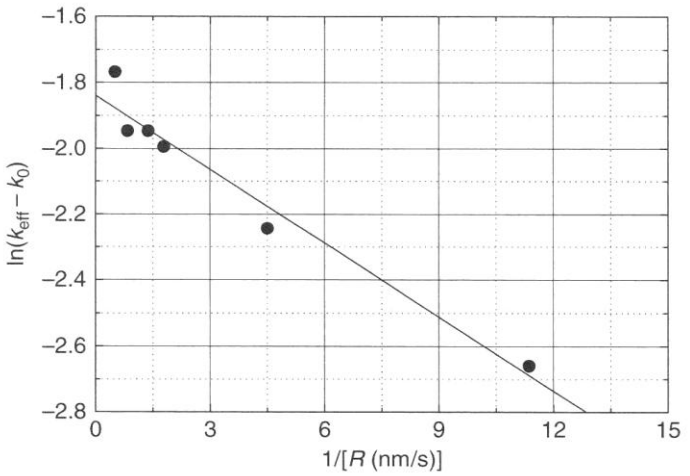

Figure 9.13 *Plot of* $\ln(k_{eff} - k_0)$ *of* Pb^{2+} *ions in* $BaNO_3$ *crystals against* $1/R$*; impurity concentration* c_i *in the solution about 10 mol%. Adapted from Tsuchiyama* et al. *(1981)*

3) Approach based on statistical selection

Voronkov, Chernov (1967):

$$k_{eff} = \frac{k_0}{1+\sigma/\sigma_{const}}, \qquad (1)$$

where: σ_{const} – constant.

When $\sigma/\sigma_{const} << 1$,

$$k_{eff} = k_0 - k_0\sigma/\sigma_{const} \qquad (2)$$

Natural statistical selection depends on kinetics of attachment and detachment of impurity particles at kinks in steps.

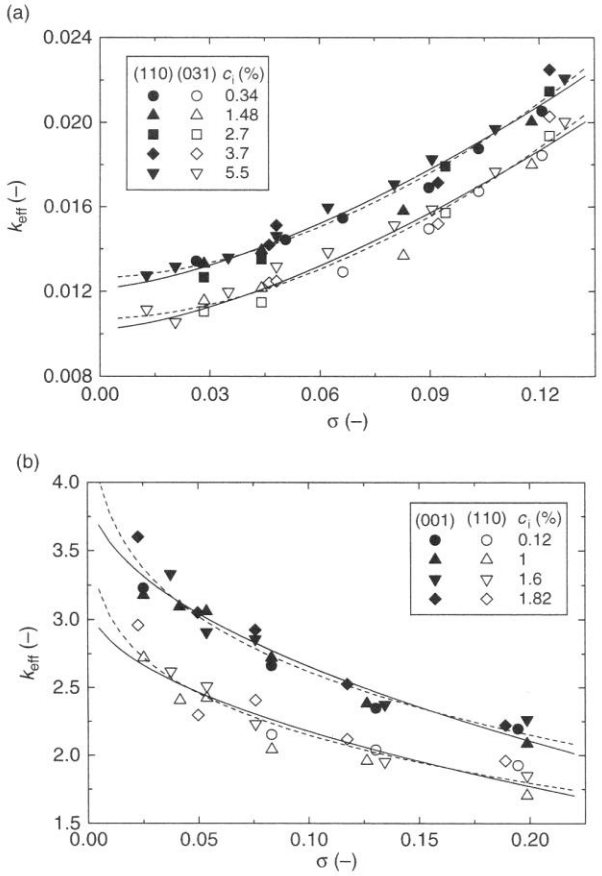

Figure 9.15 *Dependence of effective segregation coefficient k_{eff} of additive ions for two different faces of crystals grown from aqueous solutions on supersaturation σ: (a) CrO_4^{2-} ions in the (110) and (031) faces of K_2SO_4 crystals and (b) Ni^{2+} ions in the (001) and (110) faces of $ZnK_2(SO_4)_2 \cdot 6H_2O$ crystals. Curves were drawn according to Equation (9.43) with different values of n_2: (a) $n_2 = -0.5$ (continuous curve) and -0.8 (dashed curve), and (b) $n_2 = 0.5$ (continuous curve) and 0.8 (dashed curve). Original data are from Zhmurova and Khaimov-Mal'kov (1970b). Adapted from Sangwal and Pałczyńska (2000)*

4) Approach based on surface adsorption

Assumptions:

1) Impurity particles compete with particles of crystallizing substance.
2) Increase in supersaturation σ leads to increase in the density of kinks in steps.
3) $k_{eff} = k_0 + f(\text{kink density})$
$= k_0 + f_{kink}(1-\theta)/\theta$ (1)

where:

f_{kink} – fraction of kink sites on the surface of a crystal growing at supersaturation σ;

θ - total surface coverage ($\theta = \theta_{solute} + \theta_{imp}$).

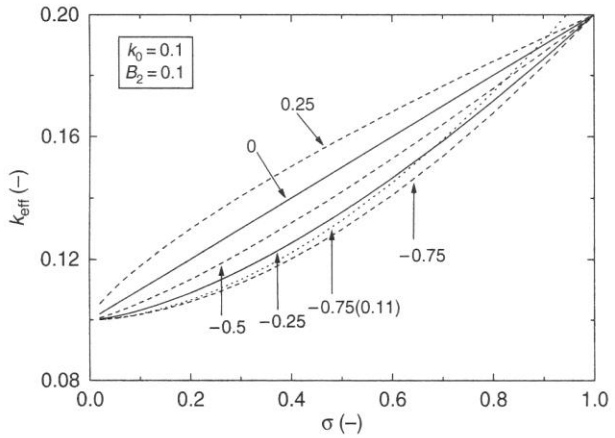

Figure 9.16 *Illustrative plots of the dependence of k_{eff} of additive in an imaginary crystal on supersaturation σ predicted from Equation (9.43) for different values of n_2 with constant $B_2 > 0$. This case represents $k_0 < 1$. Adapted from Sangwal and Pałczyńska (2000)*

For Langmuir adsorption isotherm:

$$k_{\text{eff}} = k_0 + \frac{B_1\sigma^{1-n_2}}{K_s c_s + K_L c_i} \qquad (2)$$

$$\frac{1}{k_{\text{eff}} - k_0} = C_0 + C_1 c_i \qquad (3)$$

For Freundlich adsorption isotherm

$$k_{eff} = k_0 + B_2\sigma^{1-n_2} / c_i^m, \qquad (4)$$

where:

B_1, B_2, m , C_0 and C_1 – constants;

K_s, K_i – Langmuir constants;

n_2 – a measure of barrier associated with the effect of supersaturation σ.

$$k_{\text{eff}} = k_0 + \frac{B_1 \sigma^{1-n_2}}{K_s c_s + K_L c_i} \qquad (2)$$

$$k_{eff} = k_0 + B_2 \sigma^{1-n_2} / c_i^m, \qquad (4)$$

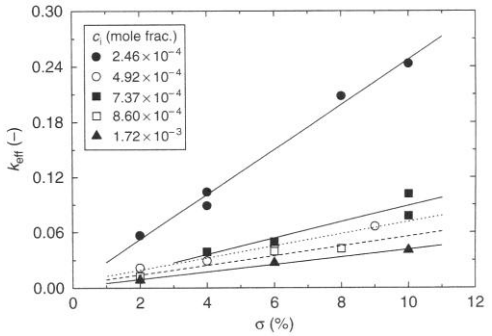

Figure 9.17 *Segregation coefficient k_{eff} of Cu^{2+} ions in AO crystals as a function of supersaturation σ for different impurity concentrations c_i. Reproduced from E. Mielniczek-Brzóska, K. Giełzak-Koćwin, and* K. Sangwal. J. Cryst. Growth ***212***, *532. Copyright (2000), with permission from Elsevier*

AO – ammonium oxalate monohydrate

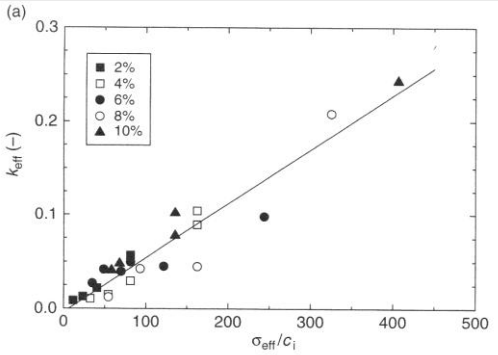

Figure 9.21 *Plots of k_{eff} for (a) Cu^{2+} and (b) Fe^{3+} in AO crystals against σ_{eff}/c_i^m. Reproduced from K. Sangwal, E. Mielniczek-Brzóska, and J. Borc.* J. Cryst. Growth ***244***, *183. Copyright (2002), with permission from Elsevier*

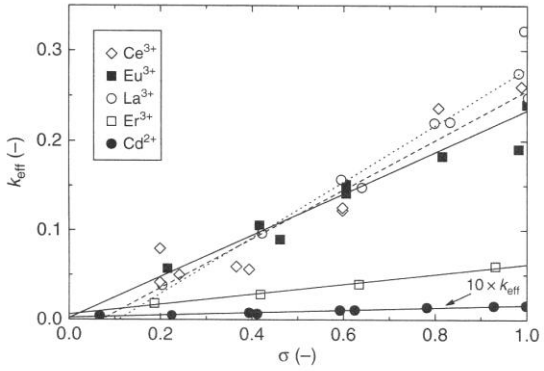

Figure 9.18 *Segregation coefficient k_{eff} of various lanthanides in gypsum crystals as a function of supersaturation σ. Impurity concentration: 3×10^{-4} M lanthanides and 4.4×10^{-4} M Cd^{2+}. Adapted from de Vreugd* et al. *(1994)*

$$\frac{1}{k_{\text{eff}} - k_0} = C_0 + C_1 c_i \qquad (3)$$

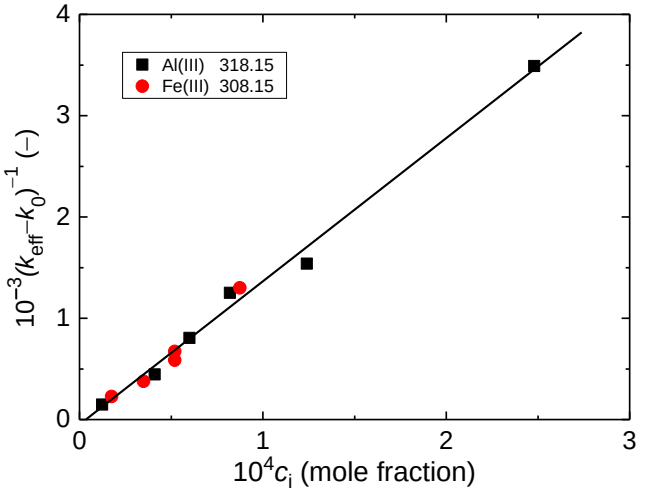

ADP – ammonium dihydrogen phosphate';
antisolvent crystallization;
Sangwal et al. JCG 614 (2023) 127235

Relationship between k_{eff} and face growth rate R

From the relation

$$R \approx A(\sigma - \sigma_c)^n,$$

$$k_{eff} = k_0 + B_2 \sigma^{1-n_2} / c_i^m,$$

one obtains

$$k_{\text{eff}} = \left(k_0 + \frac{B_2 \sigma_c}{c_i^m} \right) + \frac{B_2}{A^{1/n} c_i^m} R^{1/n}.$$

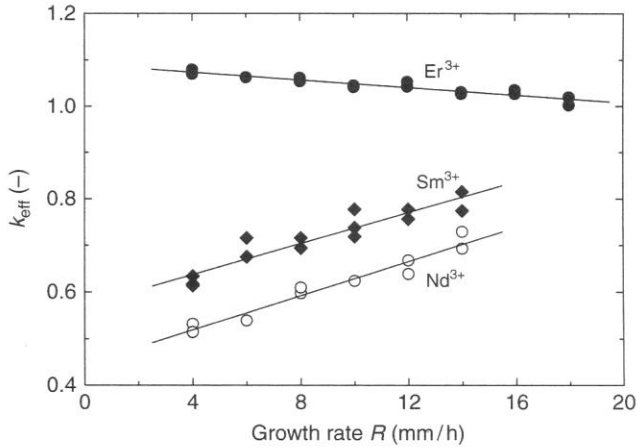

Figure 9.22 *Dependence of effective segregation coefficient k_{eff} of three rare earth ions in cubic zirconium dioxide crystals on growth rate R. The crystals were grown by the scull melting technique. Data from Römer* et al. *(1994)*

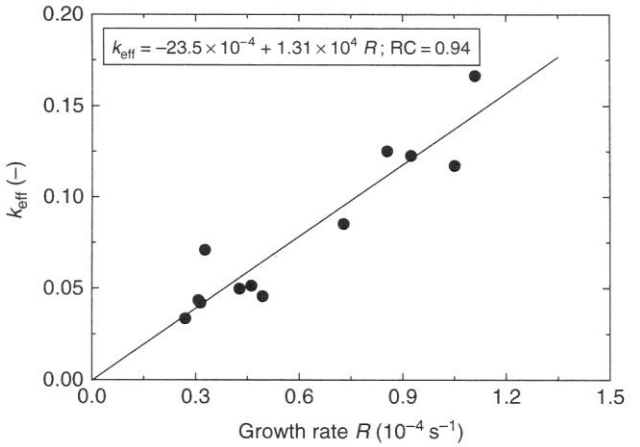

Figure 9.23 *Dependence of k_{eff} of La^{3+} ions in gypsum crystals on growth rate R. Original data from de Vreugd* et al. *(1994)*

Threshold supersaturation for capture of imputies during growth

From the plots $k_{eff}(\sigma)$, one obtains σ_0:

$$k_{\text{eff}} = p(\sigma - \sigma_0).$$

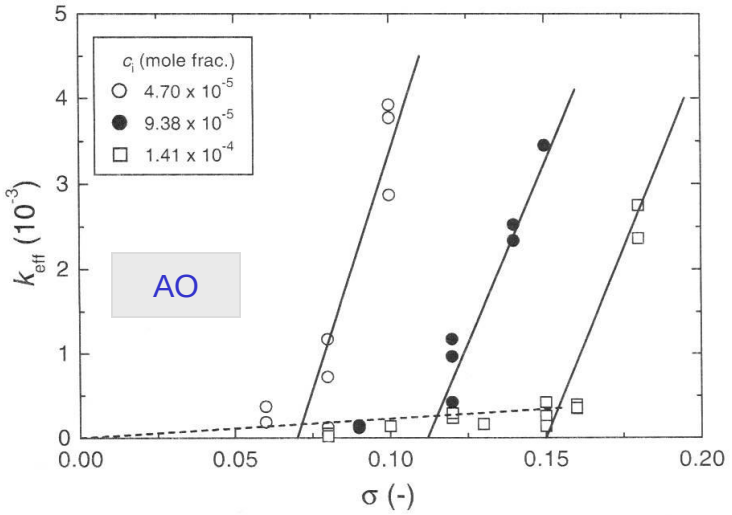

Fig. 1. Plots of k_{eff} of Mn(II) ions against σ for different c_i. Note two distinct linear dependences in the ranges of $k_{\text{eff}} < 5 \times 10^{-4}$ and $> 5 \times 10^{-4}$.

From the theory of inhibition of face growth rate by impurity, we have the dependence:

$$\frac{1}{\sigma^*} = \frac{1}{\sigma_1}\left(1 + \frac{1}{Kc_i}\right),$$

where: σ_1 – constant, K – Langmuir constant.

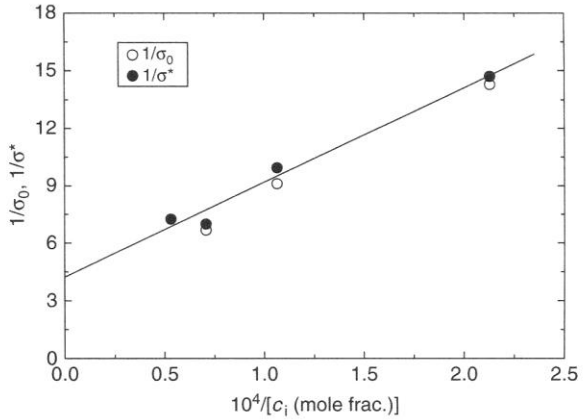

Figure 9.26 *Dependence of $1/\sigma_0$ and $1/\sigma^*$ on $1/c_i$ of Mn^{2+} impurity according to Equation (9.53). The plot was drawn for $\sigma^*(c_i)$ data. Reproduced from K. Sangwal and E. Mielniczek-Brzóska. J. Cryst. Growth **257**, 185. Copyright (2003), with permission from Elsevier*

Literature

D. Hull and D.J. Bacon, Introduction to Dislocations, 4th edition, Butterworth-Heinemann, Oxford (2001).
A.J. Dekker, Solid State Physics, MacMillan, London (1964).
C. Kittel, Introduction to Solid State Physics, 5th edition, Wiley, N.Y. (1976).
J.C. Brice, The Growth of Crystals from Liquids, North-Holland (1973).
A.A. Chernov (ed.), Modern Crystallography: Crystal Growth (Springer, 1984).
K. Sangwal, Additives and Crystallization Processes: From Fundamentals to Applications, Wiley, Chichester (2007).

Acknowlegement:
Krzysztof Zabielski for scan of figures used here.